LAWRENCE
LIVERMORE
NATIONAL
LABORATORY

LLNL-TR-704343

Final Report on Small Particle Speciation for Forensics Analysis by Soft X-ray Scanning Transmission X-ray Microscopy

J. I. Pacold, A. B. Altman, S. B. Donald, Z. Dai, M. L. Davisson, K. S. Holliday, K. B. Knight, M. J. Kristo, S. G. Minasian, A. J. Nelson, T. Tyliszczak, C. H. Booth, D. K. Shuh

October 4, 2016

Disclaimer

This work performed under the auspices of the U.S. Department of Energy by Lawrence Livermore National Laboratory under Contract DE-AC52-07NA27344.

Final Report on Small Particle Speciation for Forensics Analysis by Soft X-ray Scanning Transmission X-ray Microscopy

J. I. Pacold,[1] A. B. Altman[1,2], S. B. Donald,[3] Z. R. Dai,[4] M. L. Davisson,[4] K. S. Holliday,[3] K. B. Knight,[4] M. J. Kristo,[4] S. G. Minasian,[1] A. J. Nelson,[3] T. Tyliszczak,[5] C. H. Booth,[1] and D. K. Shuh[1]

[1]*Chemical Sciences Division, Lawrence Berkeley National Laboratory, Berkeley, CA 94720, USA*

[2]*Department of Chemistry, University of California, Berkeley, CA 94720, USA*

[3]*Materials Science Division, Lawrence Livermore National Laboratory, Livermore, CA 94550, USA*

[4]*Nuclear and Chemical Sciences Division, Lawrence Livermore National Laboratory, Livermore, CA 94550, USA*

[5]*Advanced Light Source, Lawrence Berkeley National Laboratory, Berkeley, CA 94720, USA*

Executive Summary

Materials of interest for nuclear forensic science are often highly heterogeneous, containing complex mixtures of actinide compounds in a wide variety of matrices. Scanning transmission X-ray microscopy (STXM) is ideally suited to study such materials, as it can be used to chemically image specimens by acquiring X-ray absorption near-edge spectroscopy (XANES) data with 25 nm spatial resolution. In particular, STXM in the soft X-ray synchrotron radiation regime (approximately 120 – 2000 eV) can collect spectroscopic information from the actinides and light elements in a single experiment. Thus, STXM combines the chemical sensitivity of X-ray absorption spectroscopy with high spatial resolution in a single non-destructive characterization method.

This report describes the application of STXM to a broad range of nuclear materials. Where possible, the spectroscopic images obtained by STXM are compared with information derived from other analytical methods, and used to make inferences about the process history of each material. STXM measurements can yield information including the morphology of a sample, "elemental maps" showing the spatial distribution of major chemical constituents, and XANES spectra from localized regions of a sample, which may show spatial variations in chemical composition.

The initial efforts focused on XANES spectroscopy at the uranium $N_{4,5}$ edges and the oxygen K-edge acquired from a set of uranium-bearing compounds and minerals. These data were compiled into a reference library for comparison with spectra acquired from unidentified materials. In agreement with recently published surveys of uranium species, the oxygen K-edge was found to typically be the most sensitive soft X-ray spectroscopic fingerprint for classification of unknown specimens. The studies conducted for the

remainder of the project therefore devoted a large amount of effort to collecting data at the oxygen K-edge. A library of reference uranium $N_{4,5}$-edge, oxygen K-edge, and nitrogen K-edge spectra has been acquired from common uranium materials with a soft X-ray STXM.

As the STXM methodologies were being developed with reference materials, it became imperative to conduct STXM investigations with real forensic specimens. To demonstrate the capabilities of STXM analysis on real forensic specimens, uranium powders interdicted in Victoria, Australia were obtained through a collaboration with M. Kristo of Lawrence Livermore National Laboratory (LLNL). Elemental mapping and oxygen K-edge absorption spectroscopy showed that one specimen was a highly homogeneous potassium-uranium hydrate, likely the result of a precipitation process. The second specimen was found to be primarily UO_3 with micron-scale regions of other oxide and/or hydrate species located throughout the material. In addition, the sensitivity of soft X-ray absorption spectroscopy to light elements made it possible to detect significant carbon contamination in both samples.

A second set of materials with relevance to forensics, samples of UO_2 aged under controlled temperature and humidity conditions, were obtained through an additional collaboration with L. Davisson of LLNL. Both particulate materials and thin sections extracted by focused ion beam (FIB) milling were analyzed by STXM. The oxygen K-edge spectra acquired from the particulate samples showed that each contained a range of uranium oxide species including UO_2, U_3O_7, and U_4O_9. Analysis of focused ion beam (FIB) sections revealed the formation of a surface layer of U_3O_7 on a moderately aged UO_2 crystal and the presence of a uranyl species, most likely schoepite, both at the surface and throughout the bulk of a highly aged specimen. Selected specimens were also examined by intermediate-energy XANES at the U M_4-edges thereby yielding measurements of both the bulk-averaged and spatially-resolved formation of oxidized and amorphous phases.

Lastly, a set of melt glass specimens from nuclear tests has been characterized in conjunction with K. Knight (LLNL) by hard X-ray spectroscopy, yielding indications of the rate at which each specimen cooled in addition to the, chemical speciation. These samples of glassy material generated were analyzed by STXM. Chemical imaging at the Fe $L_{2,3}$ edges has been used to determine the spatial distribution of Fe(II) and Fe(III) across the material that is indicative of the iron-uranium redox couple in the glass expected to affect the chemical state of uranium in these glasses.

An excellent attribute of the three aforementioned STXM forensics investigations above is that they have been conducted not only on realistic forensic materials, they have been performed concurrently as a proof of concept demonstrating the value of STXM information as these methodologies are being utilized by the funded projects of M. Kristo, L. Davisson, and K. Knight, all of LLNL, respectively.

The work at the Molecular Environmental Sciences (MES) Beamline STXM of the Advanced Light Source (ALS) has led to improved detection limits, sample handling, and

data acquisition/analysis procedures for STXM studies of forensic specimens. Several major advances enabling STXM of radioactive particulates have been made. Fluorescence detection techniques were developed and detection limits characterized based on the use of an Amptec single element solid state detector. A modified sample holder was employed to simplify alignment of the STXM rather than having to re-position the STXM motion stages. The detection limits and energy resolution were determined for f-electron materials and light atoms, and for most STXM investigations, the normal mode of operation in transmission is the overall preferred approach.

Sample handling methodologies have been developed utilizing STXM radioactive particle application approaches including those that are environment sensitive (air or moisture sensitive, inert, and ambient). Methods to run specimens under normal near-ambient helium pressure were utilized successfully and new methods to conduct studies under high vacuum were also developed successfully. Efforts have also included radioactive particle identification via image plate scanner (autoradiography) followed by micromanipulator transfer. A particularly useful method for STXM that has been developed and implemented is the use of radioactive FIB stubs.

The STXM presents contemporary difficulties for data acquisition from particles followed by much of the same difficulties in the overall data analysis that are similar in nature to those faced by many high throughput spectromicroscopy probes (e.g., transmission electron microscope) especially when there are constraints on instrument availability. Responding to these challenges, two new programs were developed to exploit and efficiently utilize the STXM for particle studies. The first and seminal program piggybacks on the STXM data acquisition code and provides real time spectral output as a function of position and immediate processing capabilities to guide particle investigations without the need to let the STXM data collection fully complete. It also can locate suitable particles of interest for investigation. The second program was an archival record system to keep track of data and spectra that are important when examining a large number of particles. Both of these software packages have been made available to the STXM user community and have become fast favorites.

The $M_{4,5}$-edges of the actinides that reside in the intermediate X-ray region (2-6 keV) are highly sensitive to oxidation states and when collected under special high resolution detection conditions can yield spectra that have characteristic lineshapes (signatures). There was a singular opportunity to construct and use a special low-cost detector along with the rudimentary focusing properties of ALS Beamline 5.3.1 for an overall performance assessment at intermediate energies. Measurements with intermediate energy X-rays at the uranium M_4-edge using the special detection system were found to yield valuable information, albeit with slightly less resolution than expensive detector systems, and points towards the potential and value of an intermediate energy spectromicroscopy capability in the future.

The initial investment in soft X-ray STXM spectromicroscopy for forensics has had several major successful impacts and, as a primary achievement, was shown that STXM is a uniquely-suited and complementary tool for forensics. This has been achieved by

successful technical implementation of STXM methodologies to a variety of forensic materials, primarily particles. This has been successfully translated and demonstrated with actual materials of forensic interest within the performance period. The initial investigations clearly prove that STXM can contribute meaningfully to the forensics community, not only as a research tool, but could contribute as both a regular stand-alone and complementary analytical tool. First, it is clear that STXM can contribute valuable chemical information on a spatial scale approaching the true nanoscale and captures the chemical heterogeneity of materials, particularly ideal for the case of particles. The spectral information from STXM provides rich information on the chemical nature and composition as a function of location on the 25 nm scale, of forensic samples and their matrixes as well, especially from the light atom constituents which are often key signatures towards speciation. The effort has developed new two software tools that have optimized and enabled the STXM to be efficient for the study of forensic particles.

These first and initial results demonstrate the extensive capabilities of STXM for forensics and its utility as part of the suite of nuclear forensic analysis methods. This research has aimed to take the first steps towards integrating STXM into the suite of analytical methods used for characterization and attribution of regular forensics and unidentified materials. The studies of relevant forensic materials conducted to date have established standard procedures for the use of STXM as part of a larger collaborative forensic analysis. Further technical and procedural improvements (such as the implementation of diffraction-enhanced high-resolution imaging) are expected to extend the sensitivity and range of applicability of STXM measurements to the true nanoscale of about 3 nm. Considerations for the future include studies on particle class distributions of interest with enhanced error and statistical analysis, studies of transuranic materials, and the development of dedicated synchrotron- or laboratory-based instrumentation for nuclear forensic analysis.

I. Introduction

I.A. Background

Nuclear forensic analysis is concerned with physical and chemical signatures that can provide information about the source and process history of a sample of unidentified nuclear material.[1-3] Signatures such as the presence and concentration of chemical impurities, sample morphology, and the isotopics of U, Pu, and trace elements have been identified in the literature and associated with steps in the sample history.[4-8] Sample morphology, for example, can be associated with the intended use of the material (e.g., the reactor type in the case of a nuclear fuel sample).[9] Isotopic content and trace element impurities can be correlated with process history, and in some cases can provide information on the possible geographic origin of a specimen.[10-13] Data from a broad array of analytical methods are typically needed to completely characterize a forensic specimen, with each measurement providing a different constraint on the possible process history and origin. Techniques used in the literature include mass spectrometry, nuclear counting, X-ray fluorescence, and powder X-ray diffraction.

Synchrotron radiation (SR) and light source facilities provide extraordinary capabilities for the non-destructive characterization and analysis of a range of materials by several methods that utilize photons as a probe, from the infrared to the hard X-rays. In particular, the brightness and small beams of third generation light sources have enabled X-ray microscopy techniques and have made high-resolution studies, both spectral and structural, on microscopic specimens a regular reality. For nuclear forensics, the development of the ability to safely capitalize on the availability of powerful photon-based probes such as X-ray absorption near-edge structure (XANES) and extended X-ray absorption fine structure (EXAFS) at U.S. Department of Energy Light Source User Facilities could complement the existing suite of analytical techniques used in modern nuclear forensics. The sensitivity of XANES to oxidation state lends itself, for example, to the observation of the gradual oxidation of nuclear material in storage[20] and to studies of chemical signatures of post-detonation material.[21,22] Historically, X-ray absorption spectroscopy has been applied to only a limited number of materials of forensic interest.[14-19]

The capability of X-ray absorption spectroscopy to safely work with minute, radioactive specimens is enabled by microbeams and microscopy, and is also coupled to technological improvements in sample containment and preparation. The spatial resolution of these techniques (~ 25 nm) and the chemical information available from X-ray absorption and emission spectroscopy are well-suited for the investigation of small particles, as well as heterogeneous bulk materials (with proper specimen preparation) that can be of interest in nuclear forensic studies and related research. Lastly, the access mechanisms to these capabilities as well as the future possibility of successfully transitioning X-ray spectromicroscopy methods to a laboratory-based forensics environment are important considerations.

I.B. Soft X-ray Scanning Transmission X-ray Microscopy

As forensic specimens are often heterogeneous and morphology can provide important information on process history, it is essential to use microanalytical methods, such as scanning electron microscopy (SEM)/energy-dispersive X-ray spectroscopy (EDS), transmission electron microscopy (TEM) and nanoscale secondary ion mass spectrometry (nano-SIMS).[23-28] This project has developed the use of scanning transmission X-ray microscopy (STXM) in the soft X-ray region for nondestructive nuclear forensic analysis. STXM combines 25 nm or finer spatial resolution with the nondestructive chemical sensitivity of XANES. The method yields spectroscopic data that is complementary to the elemental distributions provided by SEM/EDS and the isotopic information available from nano-SIMS. Operation in the soft X-ray regime provides access to both the actinide $N_{4,5}$-edges and the K-edges of light atoms, particularly C, N, O, and F. This is an important feature for analysis of nuclear materials since, in the case of actinide materials, the light atom edges are often more sensitive than the metal edges to variations in oxidation state and bonding.[29-32] Furthermore, relatively rapid data acquisition with soft X-rays makes it possible to avoid sample damage in most instances. Soft X-ray STXM spectromicroscopy is therefore ideal for complementing existing contemporary nuclear forensics methods.

To summarize, the capabilities of STXM include rapid determination of physical and detailed chemical characteristics with only microscopic quantities of radioactive material (due to the spatial resolution of the technique); analysis of samples with minimal handling and intrusion; the interrogation of wet or contaminated specimens; and the ability to image and speciate the matrix environment of a forensic sample, especially the light atom constituents.

I.C. Project Objectives

The primary objective of this research is to advance the technique of spectromicroscopy using soft X-ray STXM as an analytical chemistry tool for non-destructive nuclear forensics analysis. The specific tasks planned towards this objective were to (1) acquire a library of soft X-ray spectral signatures for uranium materials, (2) use fluorescence-detection mode to improve the sensitivity of soft X-ray spectromicroscopy for dilute samples, (3) extend this work to transuranic materials and matrices, particularly plutonium, and (4) improve sample preparation and data collection methodologies to achieve rapid turnaround on high-priority forensic specimens.

Tasks (1) and (2), as well as a complementary hard X-ray spectroscopy study of nuclear melt glass, were completed in 2014 and early 2015. Following the feedback from the mid-term (June 2015) Schubert Review of the project and the establishment of new uranium materials collaborations with M. Kristo and L. Davisson of Lawrence Livermore National Laboratory (LLNL), the focus of the program for the remaining period was centered on uranium materials rather than plutonium. The main experimental focus remained on the use of soft X-ray STXM spectromicroscopy for nuclear forensics, including technical developments in sample handling and data collection methodologies

at the Molecular Environmental Science (MES) STXM Beamline 11.0.2 of the Advanced Light Source (ALS), with the goal of improving utility and throughput for heterogeneous forensic specimens. In addition, hard X-ray spectroscopic results were published shortly after the Schubert Review, and a unique opportunity was taken advantage of to develop and evaluate of potential intermediate X-ray methods for nuclear forensics.

There has been less direct emphasis on the determination of error since errors involved in these measurements are standard to the STXM X-ray absorption spectroscopy technique. For specific particles this depends on the heterogeneity and on the sampling regimen for respective particle classes. In these studies, multiple specimen particles were examined to ensure correctness, however, the focus was not on the fully rigorous determination of error or statistics within the particle distributions which is beyond scope and primary objectives of this work.

II. General Program Organizational Overview

II.A. Approach

The effort has primarily focused on the development and use of soft x-ray STXM spectromicroscopy at the ALS for nuclear forensics. As described above, soft x-ray STXM utilizes the actinide N-edges, the light element K-edges from boron through silicon, and other low-lying electron energy levels to obtain speciation (oxidation states, chemical form, and coordination environment) with 25 nm spatial resolution. Developments in sample preparation, efficient data acquisition, and partially automated data analysis have been pursued, since forensic studies often have interest in rapid turnaround. This is particularly important when the same sample must be examined using a large number of different methods at different facilities.[10,11]

Another initial thrust in this project utilized hard X-ray absorption spectroscopy, both XANES and EXAFS, to examine the bulk speciation of iron, uranium, and plutonium in several nuclear melt glasses with the explicit aim of translating the bulk studies to lower energy SR measurements by STXM (to enable further speciation of iron at the L-edges with high spatial resolution). Concurrently, there has been a measured effort to evaluate the potential of intermediate energy (2-6 keV) XANES resulting from the familiarity, knowledge, and experience of the principal investigator in this unique energy regime. Coupled with recent experimental advances and results from fundamental studies that are cited in section III.D, makes a small effort in this direction worthwhile and anticipates the development of high-performance spectromicroscopy beamlines and laboratory facilities in this particular energy range that might have great impact in the field. This intermediate energy approach relies on low-cost innovative detection schemes to collect high energy-resolution signals originating from the actinide M-edges that have been shown to be extremely sensitive to actinide speciation. A longer-term priority of this program is to establish the technical basis necessary to develop instrumentation for laboratory-based, rather than synchrotron-based, X-ray microanalysis of forensic specimens to improve understanding of chemical speciation in nuclear materials.

II.B. Report Organization

This report proceeds as follows. Section III describes in more detail the experimental methods used: soft X-ray STXM, intermediate-energy XANES, hard X-ray XANES and EXAFS, sample preparation methods, and software development projects. In section IV the results of several projects are presented: baseline spectra acquired from common uranium materials; soft X-ray STXM and intermediate-energy XANES measurements on aged uranium oxides; hard and soft X-ray studies of oxidation state effects in nuclear melt glass; and the improvements in use of beam time resulting from the software development project. Section V describes future prospects for STXM-driven studies, with a view towards integrating STXM into the suite of existing nuclear forensic analysis methods. Section VI summarizes and concludes the report. A list of tables and figures is given in Appendix 1. Scientific activities conducted under this program, including publications and manuscripts being prepared, are listed in Appendix 2.

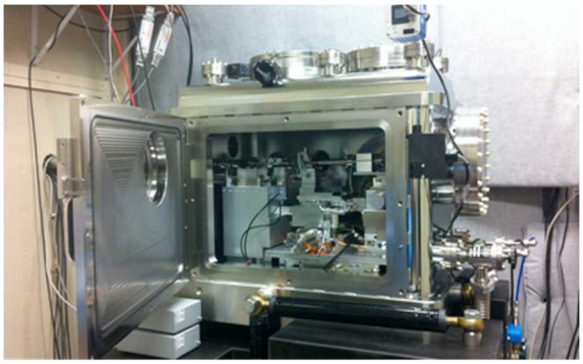

Figure 1. Photograph of current configuration of ALS-MES STXM.

III. Experimental Methods

III.A.1 Soft X-ray Scanning Transmission X-ray Microscopy

The MES STXM (Fig. 1) is located on one of the two MES Beamline 11.0.2 branchlines of the ALS at Lawrence Berkeley National Laboratory (LBNL).[33] The general design and operation principles of the STXM instruments and additional details on the MES STXM at the ALS in particular have been reported previously.[34-36] In brief, the MES beamline provides a regular operational energy range from approximately 120 eV to 2000 eV and a resolving power (E/ΔE) greater than 7500. X-ray zone plates and interferometer-controlled sample positioning stages are used to enable imaging with spatial resolution better than 25 nm. Images are usually acquired by rastering a sample through the focused X-ray beam and monitoring the transmitted intensity with a photomultiplier or photodiode. As discussed further below, a silicon drift detector may be installed to acquire X-ray fluorescence images. Stacks of images collected over a range of photon energies can be processed to extract spatially resolved spectroscopic data.

The ALS electron storage ring and the MES beamline operate under ultra-high vacuum (UHV), but the STXM instruments at the ALS can operate under vacuum (approximately

10^{-7} Torr) or He at ambient pressure, as the photon beam enters each microscope through a 50 nm Si_3N_4 isolation window. Consequently, it is not necessary to prepare samples for compatibility with vacuum, and sample changes are relatively rapid. To operate at ambient pressure, the microscope chamber is typically purged with helium prior to data collection to prevent attenuation of the soft X-ray beam.

III.A.2 STXM in Fluorescence-Detection Mode

An improved ability to discriminate against interfering signals in transmission detection, to enhance the signal sensitivity of STXM spectromicroscopy, and to enable the examination of more bulk-like materials has been developed by deploying a dispersive single element solid state fluorescence detector in the MES STXM (Fig. 2). Together with the scientific staff of the MES Beamline, we have implemented and tested a new sample holder with radioactive materials that permits a much easier and more regular implementation of fluorescence detection mode. Several further detailed tests of fluorescence detection sensitivity were conducted to establish sensitivity and signal to

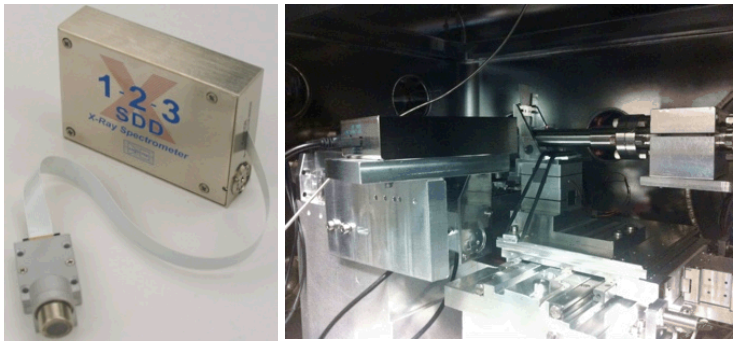

Figure 2. Left: solid state fluorescence detector (Amptek SSD) used for soft X-ray spectromicroscopy with the MES STXM. Right: mounting of the detector with respect to a STXM sample holder.

background ratio trade-offs. The energy resolution of the detector (125 eV) is sufficient to separate the K-edge signals from oxygen and nitrogen, enabling K-edge spectroscopy of light atoms at concentrations of 0.5% – 1.0% by weight. It is also possible to detect lanthanides and transition metals at lower concentrations. A conservative estimate of the detection limit is 0.05 wt% for transition metals detected by L-edge derived fluorescence. Note that fluorescence yields are typically higher in the hard X-ray regime than in the soft X-ray regime, and consequently the detection limit for XRF is still somewhat lower than for fluorescence-detector-coupled STXM.

III.B.1 Standard sample preparation methods

Preparing most particulate specimens for STXM analysis requires minimal processing. Experiments with dispersible radioactive materials (such as particulates) require the use of two Si_3N_4 windows sealed together to contain the sample. Typically, a microgram (or less) quantity of material is enclosed between the windows; consequently, sample activities are typically less than 1 pCi and no radioactive material is exposed to UHV. To

ensure compatibility with the penetration depth of soft X-rays (on the order of 100 – 500 nm for most actinide materials), coarse samples may be pulverized in a mortar and pestle before mounting.

III.B.2 Focused Ion Beam Milling

More recently, several analyses have been conducted on thin sections of material prepared by focused ion beam (FIB) milling.[37] This process results in specimens with ideal thickness for STXM (typically 100-200 nm) and, unlike mechanical grinding, preserves the spatial organization of the material. Typically, high-quality spectra can be obtained from these specimens, and it is straightforward to distinguish, for example, between regions corresponding to the surface and bulk of the original material. Samples have been provided by LLNL prepared using and dual beam FEI Nova600i, and, more recently, prepared by the LBNL team at the California Institute for Quantitative Biology (QB3) Berkeley Nanotechnology Center's FIB (dual beam FEI Quanta) at UC Berkeley, which is compatible with radioactive materials.

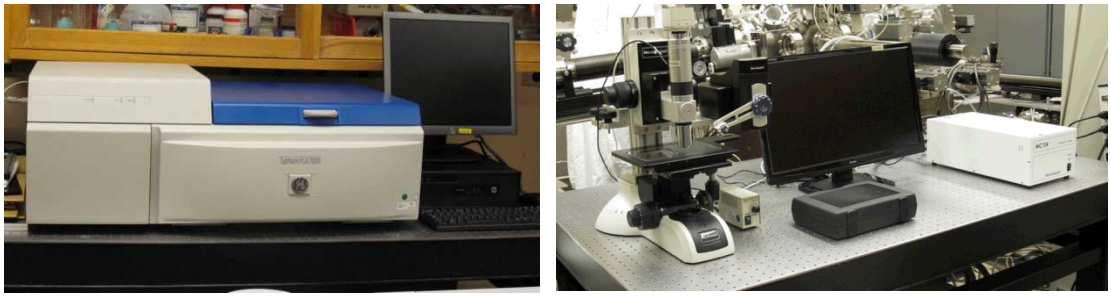

Figure 3. Photograph of particle picker system; image plate scanner (left) and particle picking microscope (right).

III.B.3. Micromanipulator and Autoradiography

Another common scenario in terms of sample handling is to examine particles that have been selected from many others via alpha-radiation fission track or gamma image plate detection. LBNL has acquired a particle picking system (Fig. 3) that is a combination of a GE Healthcare Life Sciences Typhoon image plate laser scanner (FLA7000) and a MicroSupport Sampling Microscopy Station with MicroTweezers and MicroInjector particle handling systems. Vibration isolated worktops for the two systems were obtained (supported from another source). Test experiments with the respective systems have been conducted to gain experience prior to use with loose radioactive particulate materials. The initial experience with this system spurred the development of an improved apparatus. The design for an effective gridded titer plate from which particles can be segregated and retrieved with relative ease has been completed, and awaits fabrication followed by testing. This effort has been slowed in favor of FIB preparation and analysis of LLNL specimens, even though sample handling and related procedures continue to be a priority.

III.C. Data Acquisition and Analysis Software Development

For studies of heterogeneous particulate materials, and for cases where sectioning or other mechanical processing is impossible, a software-assisted STXM data acquisition protocol has been developed. Typically, the process of collecting STXM data begins with a survey of a mm-scale area of sample at coarse resolution (> 10 microns). The user then selects regions of the sample with areas on the order of 50 × 50 microns for imaging at sub-micron resolution. Finally, smaller regions (on the order of 10 × 10 microns) are selected for imaging and spectromicroscopy at resolutions ranging approximately between 25 nm and 100 nm. The choice of a particular region for inspection at high resolution depends on the presence of the element of interest and the optical density of the material (optical densities higher than approximately 1 at the absorption maximum lead to distortion of the spectrum). The process of searching for an appropriate region varies considerably depending on sample morphology and operator experience, and several hours of beam time may be required to manually locate a suitable particle.

With this in mind, a software tool was developed to streamline the process of surveying a heterogeneous sample by identifying regions of a coarse-resolution image that are likely to contain small particles (based on the distributions observed in past samples). Testing of this software has been carried out at the ALS-MES STXM and the Canadian Light Source 10ID-1 STXM. More recently, extensions to this code have been developed to automatically generate easily-readable log files summarizing data collection on one sample, and to attempt to identify specimens by comparing their soft X-ray absorption spectra with user-provided reference data. The envisioned forensic application of this software tool extension is to aid in the rapid analysis of unidentified forensic samples by comparing spectral fingerprints with, for example, the reference library described in section IV.A that is one of the major goals of STXM spectromicroscopy project.

III.D Intermediate-Energy XANES

The $M_{4,5}$ edges of the actinides are highly sensitive to oxidation state. For example, the chemical shift in the uranium M_5 edge between U(IV) and U(VI) is approximately 2.5 eV, compared to less than 0.5 eV for the N_5 edge and approximately 2 eV for the L_3 edge. The actinide M edges fall in the "intermediate-energy" regime between soft and hard X-rays (approximately 3-5 keV), where most synchrotron radiation beamlines cannot operate efficiently, and as a result have historically not been investigated as frequently as the N and L edges. However, several notable uranium M-edge studies have appeared in recent years,[38-41] as intermediate-energy beamline and instrumentation development efforts have progressed at several light sources. Beamline 5.3.1 of the ALS provides approximately 10^{11} photons/second at the uranium M_4 edge (3.7 keV), which is sufficient for XANES and X-ray emission spectroscopy (XES) studies.

A new compact XES instrument (Fig. 4) was designed and commissioned for this work. This to added a new capability for these types of investigations and provided baseline information for the utilization of XES in this field. Importantly, the results portend how an intermediate energy system might be successfully implemented in a laboratory

environment, spatially-resolving or not based on an XES detection scheme. The instrument consists of an array of flat Si (220) crystals positioned so that each crystal disperses uranium Mβ radiation over part of a position-sensitive X-ray detector. Similar instruments were previously deployed at the Advanced Photon Source for hard X-ray experiments.[42,43] In combination with a detector optimized for intermediate-energy detection, this arrangement made it possible to acquire a low-noise U Mβ spectrum in approximately 10 minutes. A series of emission spectra collected at different monochromator energies could then be combined to extract high-resolution XANES (HR-XANES) data. This approach suppresses the intrinsic broadening observed in X-ray

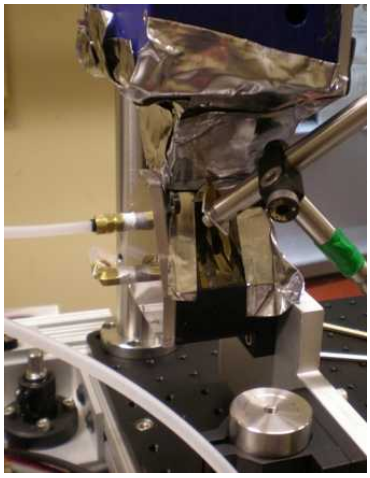

Figure 4. Intermediate-energy X-ray emission spectrometer at ALS Beamline 5.3.1.

absorption spectroscopy due to the short lifetime of the core holes created by the incident X-rays.[40,44] In the resulting spectra (see section IV.D and reference 40), the spectral features of the uranium M_4 edge are more pronounced, allowing a more accurate determination of the oxidation states present in the sample.

III.D Hard X-ray XANES/EXAFS

XANES in the hard X-ray regime is a well-established method for nondestructive determination of metal oxidation states. For sufficiently concentrated samples, collecting data in the EXAFS region can make it possible to determine the coordination of the targeted atom.[44-46] This approach provides bulk-averaged or micron-scale information on the metal atoms in a sample, and is therefore complementary to the submicron-scale data on light atom bonding provided by soft X-ray STXM.

Hard X-ray absorption spectroscopy measurements for this project were carried out at beamline 11-2 of the Stanford Synchrotron Radiation Lightsource (SSRL). Each sample was typically ground into powder with a mortar and pestle, and then either applied to polyimide tape to generate a uniform layer 1-5 microns thick, or (for more dilute samples) packed into aluminum cells with internal volumes of approximately 2.5 mm^3. During data collection, samples were placed in a liquid He cryostat. X-ray absorption data were acquired in transmission mode by measuring the photon flux immediately before and after the sample with ion chambers. In the case of dilute samples, fluorescence-mode spectra were acquired with a 100-element Ge detector.

IV. Results

IV.A. Library of Reference Uranium Material Spectra

Uranium $N_{4,5}$ edge and oxygen K-edge absorption spectra have been acquired from a range of naturally occurring and industrially significant uranium-bearing compounds and minerals (Fig. 5 and Table 1). These materials were selected to cover as broad a variety as

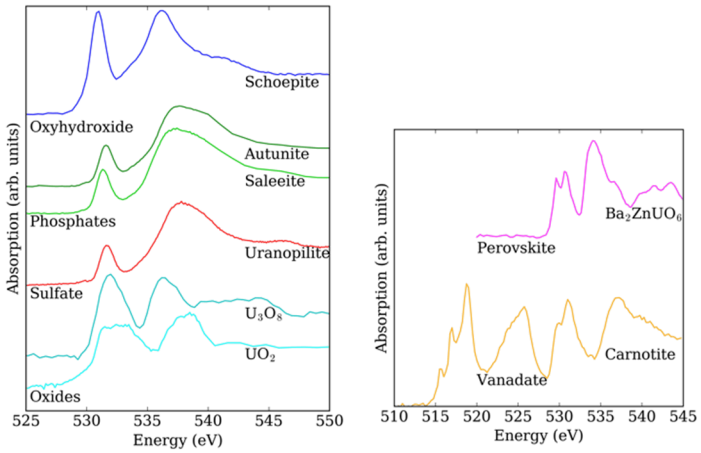

Figure 5. Oxygen K-edge spectra acquired from representative standard uranium materials.

Table 1. Uranium materials used to compile a library of soft X-ray absorption spectra.

Material	**Spectra acquired**
U metal	U $N_{4,5}$
UO_2	U $N_{4,5}$; O K
U_3O_8	U $N_{4,5}$; O K
UN	U $N_{4,5}$; N K
UN_2	U $N_{4,5}$; N K
UH_3	U $N_{4,5}$
UF_4	U $N_{4,5}$; F K
UF_5	U $N_{4,5}$; F K
US_2	U $N_{4,5}$; S $L_{2,3}$
UO_2F_2	U $N_{4,5}$; O K; F K
UO_2SO_4	U $N_{4,5}$; O K
UO_2Cl_2	U $N_{4,5}$; O K
$UO_2(CN)_5$	U $N_{4,5}$; C K; N K; O K
UO_2(BBP)	U $N_{4,5}$; C K; O K
UO_2(SCN)	U $N_{4,5}$; C K; N K; O K
Ba_2ZnUO_6	U $N_{4,5}$; O K
Schoepite, $(UO_2)_8O_2(OH)_{12}$•$12(H_2O)$	U $N_{4,5}$; O K
Saleeite, $Mg(UO_2)_2(PO_4)_2$	U $N_{4,5}$; O K
Carnotite, $K_2(UO_2)_2(VO_4)_2$	U $N_{4,5}$; O K; V $L_{2,3}$
Autunite, $Ca(UO_2)_2(PO_4)_2$•$12H_2O$	U $N_{4,5}$; O K; Ca $L_{2,3}$
Uranopilite, $(UO_2)_6SO_4(OH)_6O_2$•$14H_2O$	U $N_{4,5}$; O K

possible of ligands and uranium bonding environments. In agreement with other soft X-ray surveys of uranium materials,[47] the uranium N edges show small chemical shifts correlated with changes in the oxidation state of uranium; further analysis has shown that the branching ratio (i.e., the ratio of intensities of the N_4 and N_5 peaks) is also correlated with oxidation state. The oxygen K-edge spectra show variations in peak location and intensity that make it possible to group specimens by ligand.[30]

IV.B. Interdicted Uranium Materials

A STXM study of interdicted uranium materials was conducted to illustrate the applicability of STXM to analysis of illicitly trafficked radionuclide substances. In a 2009 incident in Victoria, Australia, law enforcement officers seized two containers of unidentified uranium materials. Teams at the Australian Nuclear Science and Technology Organization (ANSTO) and LLNL conducted analyses of the materials, and results of the combined analysis have recently been published.[10,11] X-ray diffraction data indicated that one sample was similar to $K_2(UO_2)_3O_4 \bullet 4H_2O$, while the second was predominantly $UO_3 \bullet 2H_2O$. Isotopic analyses were used to deduce that both materials had been used as feedstocks for Pu production. Since there are no facilities in Australia consistent with the inferred process history, the analysis concluded that both materials were imported. Aliquots of each material (Fig. 6) were provided by LLNL for analysis at the ALS-MES STXM. The potassium compound (a yellow powder that turned orange when heated at 750 °C for 12h) will be referred to as specimen 1 in the following discussion. The uranium oxide material (dark green powder) will be referred to as specimen 2. The materials placed on silicon nitride membranes with no further preparation.

STXM imaging of specimen 1 (Figs. 7-8) showed that the untreated material consisted of grains typically 1 micron or less in diameter. Grains of the heated material tended to form larger aggregates. Both the untreated and heated samples were chemically homogeneous. This was demonstrated by elemental mapping (Figs. 7-8), which showed that the distributions of the constituent elements were all highly correlated, and by acquiring O K-edge spectra from several grains in each sample (Fig. 9). A clear difference between the as-received and heated samples was observed in the oxygen K-edge spectra due to the dehydration process, but no significant variations were measured within each sample.

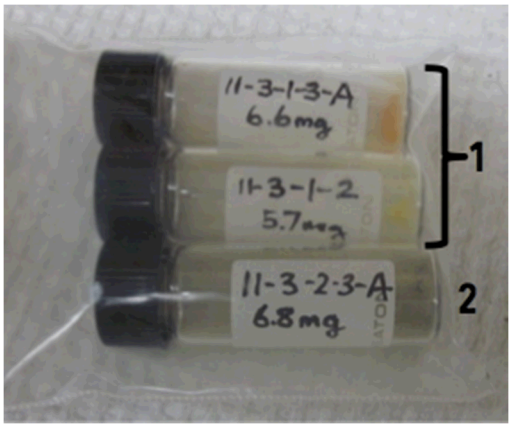

Figure 6. Interdicted uranium materials as received from LLNL.

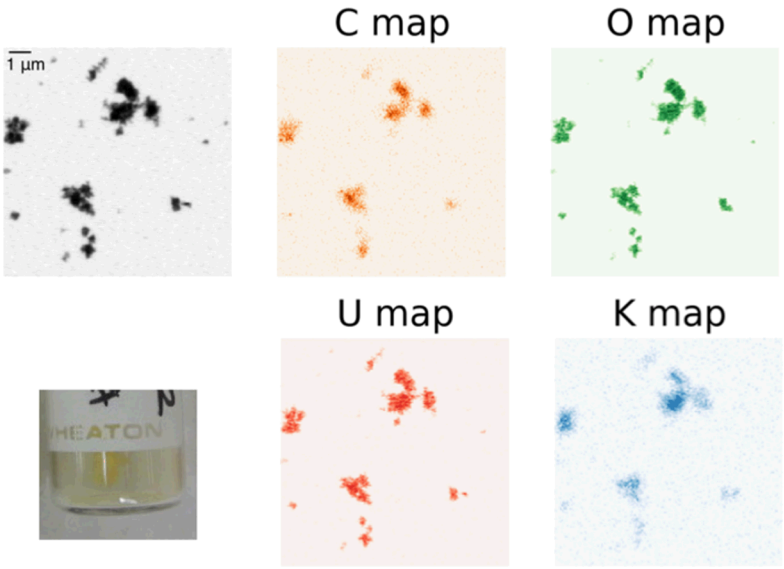

Figure 7. Normal contrast image and elemental maps acquired from interdicted specimen 1 (as-received at LLNL).

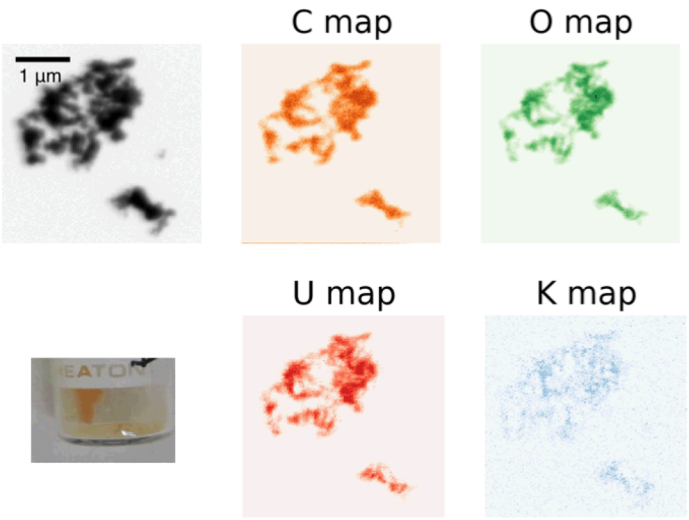

Figure 8. Normal contrast image and elemental maps acquired from interdicted specimen 1 (following heating at 750 C for 12 hours, during analysis at LLNL).

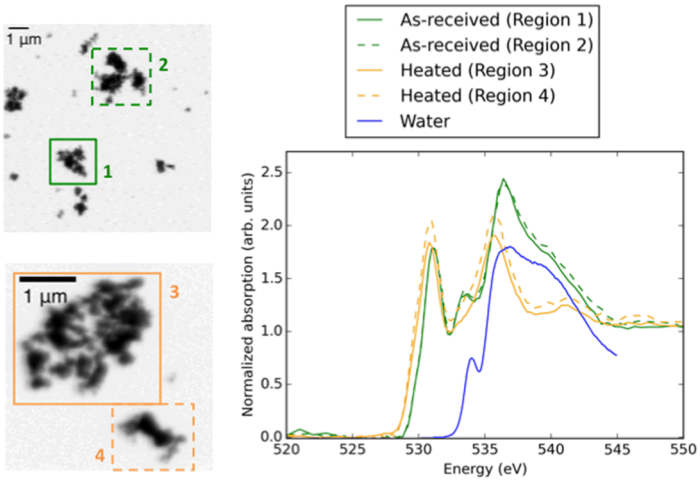

Figure 9. Oxygen K-edge spectra acquired from representative regions of the as-received and heated aliquots of specimen 1.

Specimen 2 consisted of micron-sized grains (Fig. 10) that showed considerable variation in chemical state, as demonstrated by the oxygen K-edge spectra acquired from representative grains (Fig. 11). While the bulk-averaged spectrum was consistent with a hydrated form of UO_3, in agreement with the published analysis, individual grains showed spectra that indicated either varying levels of hydration (ranging from $UO_3 \bullet 0.5H_2O$ to $UO_3 \bullet 1.3H_2O$) or varying oxidation state (possibly due to the presence of some U_3O_7). Attempting to decompose the spectra into linear combinations of reference material spectra results in relatively poor fits, and consequently the exact uranium phases present are difficult to identify with this approach. It is possible, however, to perform a principal component analysis of the spectra in order to spatially map variations in the uranium species. The decomposition (Fig. 12) gives a first principal component that is consistent with UO_3. The weight of the second principal component can then be interpreted as a measurement of the concentration of species other than UO_3. Mapping the weight of the second principal component across the specimen shows that there are submicron-scale variations in the composition of the material (Fig. 12d).

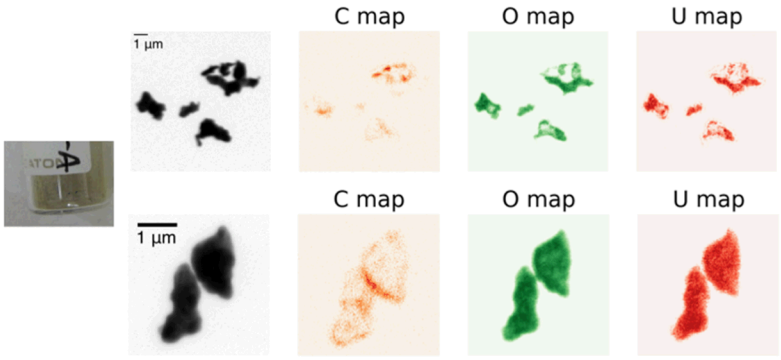

Figure 10. Normal contrast image and elemental maps acquired from two regions of interdicted specimen 2.

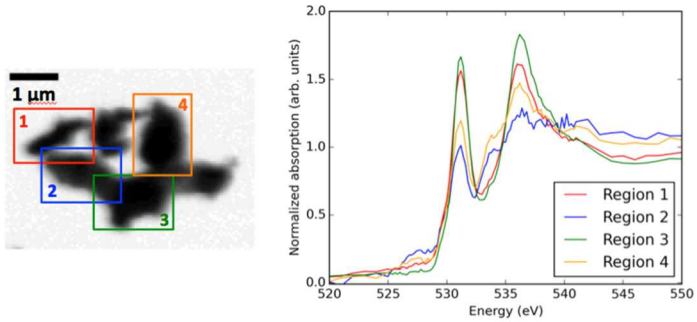

Figure 11. Oxygen K-edge spectra acquired from representative regions of specimen 2.

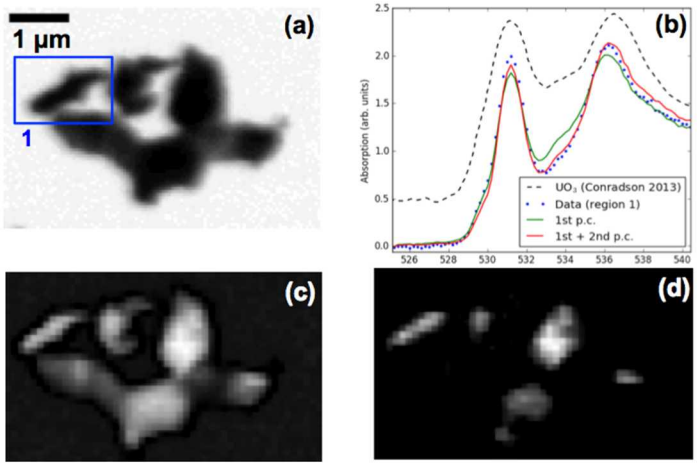

Figure 12. (a) Normal-contrast image of grains from specimen 2. (b) Results of principal component analysis of oxygen K-edge spectra acquired over the region shown in (a); the first principal component is similar to a previously reported UO_3 spectrum. Good agreement with the spectrum from a single grain, region 1 in (a), is obtained by including the second principal component. (c) Weight of the first principal component across the image. (d) Weight of the second principal component.

In addition, the elemental maps (Figs. 7-8 and 10) show a significant amount of carbon present in each sample, which was not detected in the previously reported mass spectrometry measurements. The estimated composition of each specimen is given in Table 2. Both the carbon contamination and the variations in hydration or oxidation state across specimen 2 are indicative of long-term storage under poorly controlled conditions. A systematic study of these effects is described in section IV.C.

Table 2. Compositions of interdicted specimens.

Specimen	Formula	U at%	O at%	C at%	K at%
1	$UO_{3.4}C_{0.1}$	22	76	2	---
2	$UO_{3.25}C_{0.5}K_{0.25}$	20	65	10	5
2 (heated)	$UO_{2.73}C_{0.73}K_{0.09}$	22	60	16	2

These results show that STXM as a stand-alone method can provide information on the chemical state and compositional homogeneity of a forensic specimen, using small quantities of material and minimal sample preparation. Here, the spatially resolved chemical state information derived from STXM, and its sensitivity to carbon and other light elements not detectable by mass spectrometry, can be used to determine forensic information about the process histories of each sample that are inaccessible by most other conventional methods such as XRD and ICP-MS. Some limitations of this technique include the low sensitivity in transmission mode to trace elements, and, in some cases, uncertainties in determining stoichiometry due to interferences between neighboring electron energy levels (e.g., in this case, the proximity of the potassium L edges and the carbon K edge made it difficult to determine the C:K ratio in specimen 1). These limitations can be addressed by using STXM in conjunction with existing, established methods such as X-ray fluorescence and mass spectrometry.

IV.C Aging Effects in Uranium Oxides

Uranium dioxide is known to form surface layers of other oxide species over days to weeks of exposure to atmospheric oxygen and water vapor.[48-52] Prolonged exposure can lead to bulk transformation of the material to, for example, U_3O_7, U_3O_8, intermediate oxides (UO_{2+x}), and/or hydrated uranium species. These processes have been studied primarily because of their relevance for long-term storage of nuclear fuel, but are also of interest from a forensic point of view as they provide a possible signature of the history of an unidentified sample. STXM analysis has been applied to several specimens of UO_2 aged under controlled conditions, both in native (particulate) form and as thin sections prepared by FIB milling (see section III.B.2).

Stoichiometric UO_2 was prepared by reductive methods and aliquots were aged at several levels of 34%, 56%, and 98% relative humidity (RH) for 378 days. Some of the material aged at 98% RH was removed 90 days into the aging process, and a FIB section 100 nm thick was prepared from this material. At the end of the 387-day period, a second FIB section was taken from the material aged at 98% RH. Each FIB lamella was mounted on a copper grid for TEM analysis, and was left in place on the grid for STXM measurements. Separately, several particles from each sample of aged material were deposited on silicon nitride windows with no further processing.

Oxygen K-edge spectra acquired from several representatives of the particulate samples are shown in Fig. 13. There is significant variation among particles, with species including UO_2, U_4O_9, and intermediate oxides present regardless of the level of relative humidity used. This result emphasizes the need for both bulk-averaged spectroscopy and microanalytical methods applied to a statistically significant number of particles to obtain

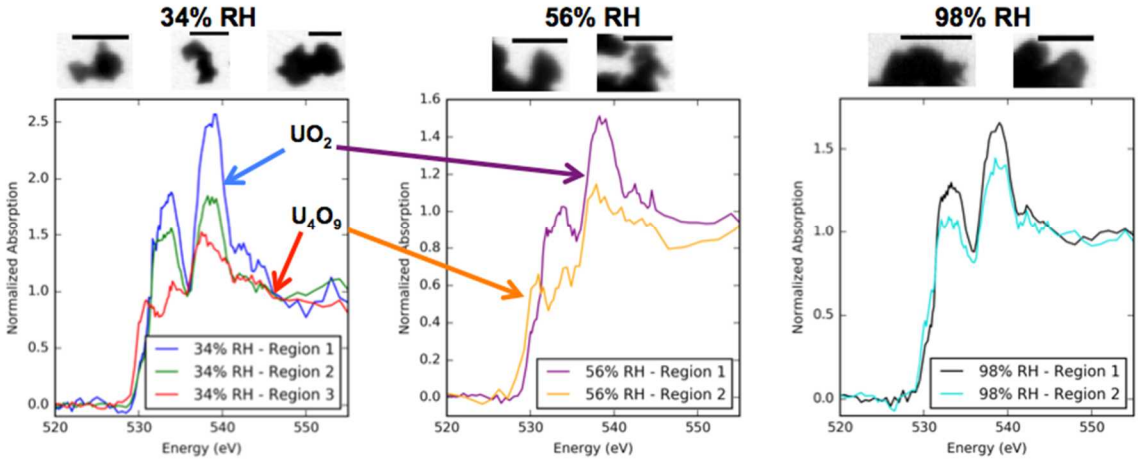

Figure 13. Images and oxygen K-edge spectra acquired from samples of UO_2 aged at various levels of relative humidity for 378 days. All scale bars are 1 micron.

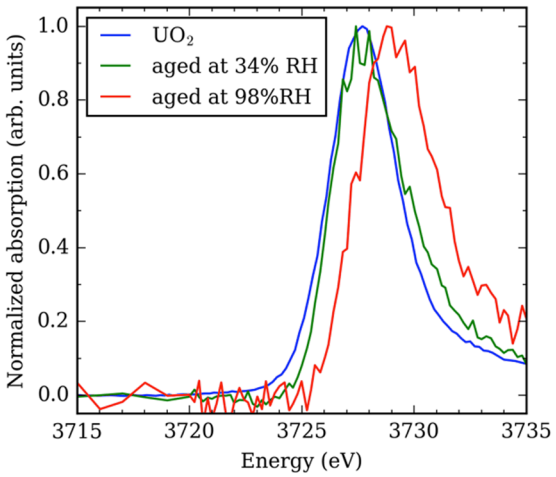

Figure 14. High-resolution U M_5-edge XANES spectra acquired from a reference uranium oxide powder and aged UO_2 samples. The ~2eV chemical shift in the absorption edge of the sample aged at 98% humidity indicates almost complete oxidation to U(VI).[41]

a complete characterization of an aged specimen. In this case, bulk-averaged oxidation states were estimated by acquiring high-resolution XANES data at the uranium M_5 edge from each particulate sample (using a beam focused to a spot approximately 50 microns in diameter). The absorption spectra (Fig. 14) show clear oxidation from U(IV) towards U(VI) with increasing humidity.

The availability of the FIB sections made it possible to acquire detailed quantitative maps of spatial variations in uranium speciation. Fig. 15 shows STXM images of the FIB section extracted after 90 days of aging, and Fig. 16 shows a series of oxygen K-edge spectra acquired along a line extending from the surface of the material into the bulk. A clear progression can be observed starting from a 0.1-micron thick layer of oxidized Pt at the surface (applied during the FIB process), followed by a layer of a U_3O_7-like species approximately 0.2 microns thick, and finally a transition to stoichiometric UO_2 in the bulk material.

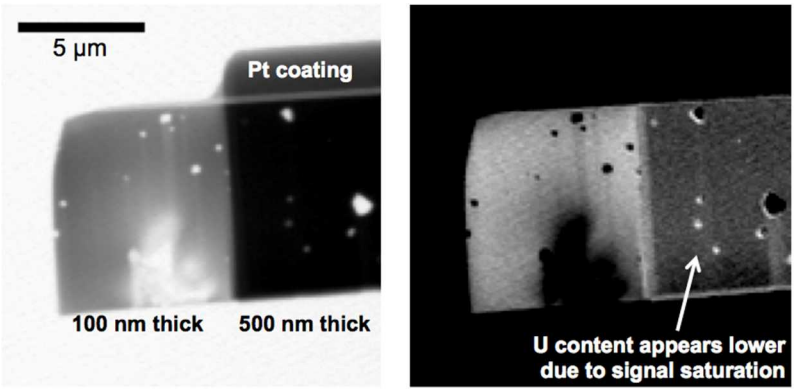

Figure 15. Normal contrast image (left) and uranium map (right) of a FIB section extracted from UO_2 aged for 90 days at 98% relative humidity. Note that a layer of Pt was applied during the FIB process.

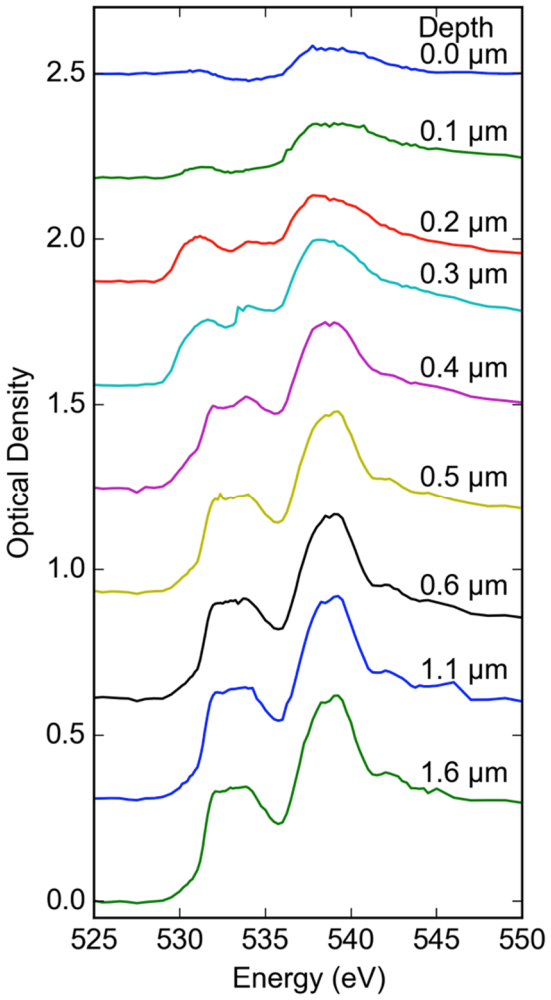

Figure 16. Oxygen K-edge spectra acquired from the FIB section shown in Fig. 12 at several depths from the surface.

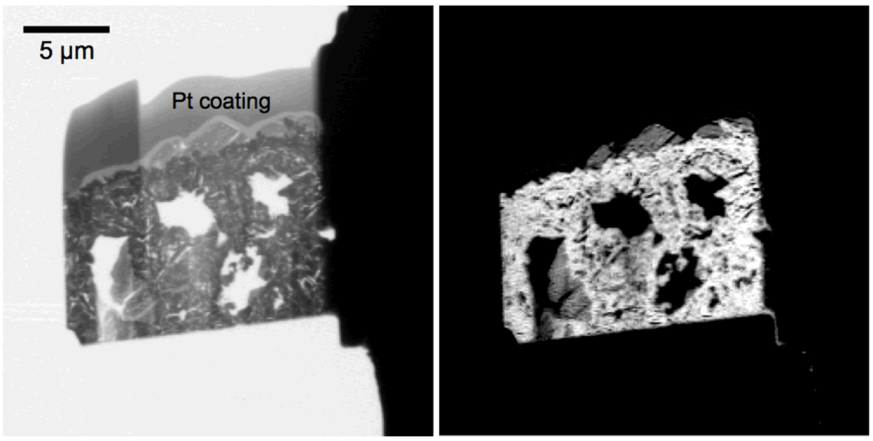

Figure 17. Normal contrast image (left) and uranium map (right) of a FIB section extracted from UO_2 aged for 378 days at 98% relative humidity.

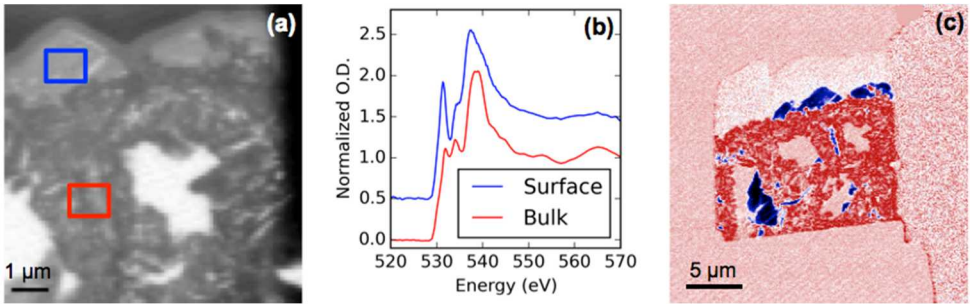

Figure 18. Spectromicroscopic analysis of the FIB section shown in Fig. 14. (a) Detail of Fig. 17(a). (b) Oxygen K-edge spectra acquired from near-surface and bulk regions indicated in (a). (c) False-color image colored by the intensity of the absorption peak at 531 eV.

Figs. 17 and 18 show the results of a similar analysis of the FIB section extracted after 378 days of aging. Here, the bulk material has clearly become heterogeneous (Fig. 17). Oxygen K-edge spectra acquired over the sample area fall into two categories. One spectral signature, observed primarily near the surface of the material, displays a prominent pre-edge peak characteristic of [$U(VI)O_2^{2+}$] materials. In this case, previous TEM electron diffraction analysis indicated that the material in these regions is amorphous; a likely candidate for its composition is amorphous schoepite. The other type of spectrum is similar to that of UO_2, but shows a splitting in the pre-edge peak that indicates some oxidation towards U_3O_7. The pre-edge feature can be used to map both phases across the entire sample (Fig. 18c).

IV.D. Nuclear Melt Glass

"Post-detonation material," i.e., fallout and debris produced by the detonation of a nuclear weapon, is an important category of materials of interest for nuclear forensics. Analysis of melt glass and other fallout is expected to carry information about the design and composition of the detonated device.[53] While there have been extensive studies of the environmental effects of weapons testing and the subsequent dispersal of radionuclides,[22,55] there have been relatively few studies of test fallout using modern

methods to improve understanding of key chemical processes such as chemical speciation.[21,54,56-59]

A bulk-averaged hard X-ray spectroscopy study of several melt glass samples from historic nuclear tests has been recently reported.[60] Hard X-ray XANES and EXAFS were used to obtain information on the oxidation state and coordination of U and Fe in each sample. Here, Fe is of interest as it is the most concentrated redox-sensitive metal in the samples, and is expected to influence the oxidation states of U and Pu; specifically, in synthetic melt glasses and vitrified nuclear waste forms, Fe is known to act as a buffer for U and Pu.[61-63] Glass generated by three test events was collected for X-ray analysis. "Event 1" melt glass is derived from a primarily U-fueled event containing some Pu. A sample of melt glass was collected by drilling into the fractured rock chimney. "Event 2" melt glass is derived from a near-surface event, primarily Pu-fueled and containing some U. "Event 3" melt glass is from a near-surface, primarily U-fueled event. Samples of local soils were also collected from the areas near Events 2 and 3, away from the ground zero and the area affected by the fallout plume at each location.

The chemical shifts observed in the XANES data show that the uranium in each device, assumed to be initially metallic U, was oxidized to a mixture of U(IV) and U(VI) (Fig. 19). The environmental Fe(III) found in the soils was almost entirely reduced to Fe(II) in the glasses (Fig. 20). U(V) can be a stable oxidation state in silicate glasses;[61,64] in this case, however, the presence of U(V) in the Event 1 and Event 3 glasses was ruled out by collecting U L_3-edge EXAFS data. EXAFS fitting (Fig. 21) showed that the bond lengths of the U species present were most consistent with U(VI) in a uranyl-like coordination and 4-coordinate U(IV).

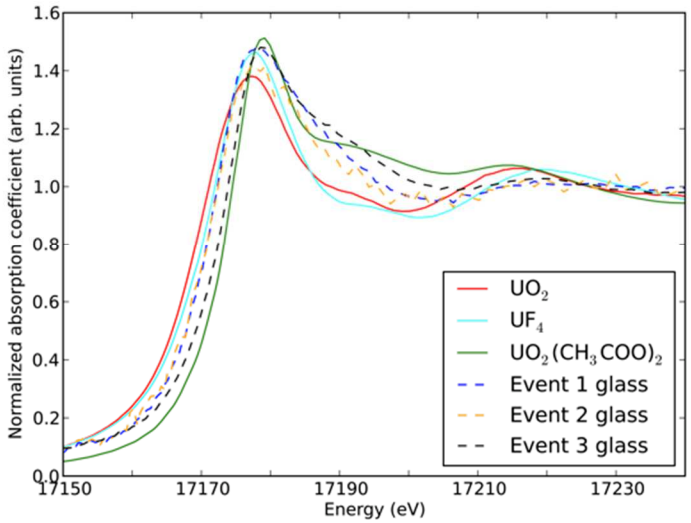

Figure 19. U L3-edge XANES acquired from melt glass specimens and reference U materials. By interpolating between the positions of the peaks corresponding to the U(IV) and U(IV) standards UO_2 and $UO_2(CH_3COO)_2$, it is possible to estimate the average oxidation state of uranium in each melt glass specimen (+4.6 for the Event 1 glass; +4.7 for the Event 2 glass; and +5.7 for the Event 3 glass).

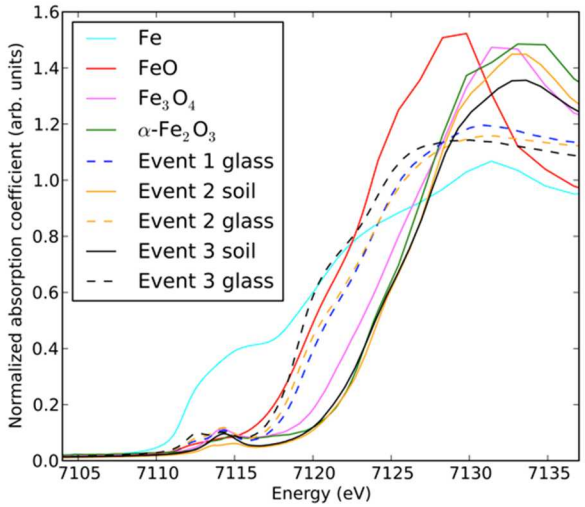

Figure 20. Fe K-edge XANES acquired from melt glass specimens and reference Fe materials. By interpolating between the positions of the Fe K edge at half-height for FeO and Fe_2O_3, it is possible to estimate the average oxidation state of Fe in each material (+3.0 for the soils; +2.2 for the Event 1 glass; +2.1 for the Event 2 glass; and +1.9 for the Event 3 glass).

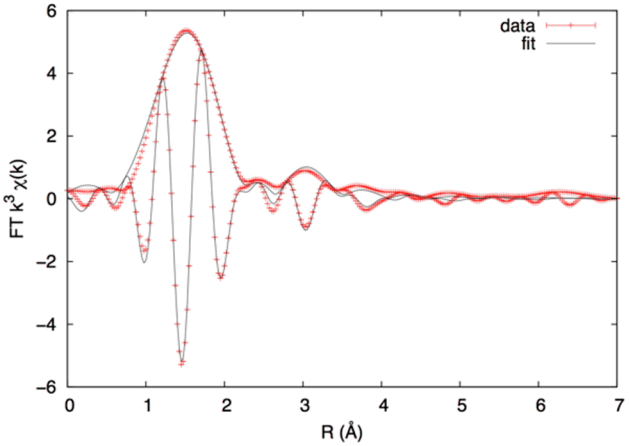

Figure 21. Fourier-transformed U L_{III}-edge EXAFS data and fit results for the Event 3 melt glass. The fit results indicate that ~60% of the uranium in the specimen is in uranyl-like coordination; more details are given in ref. 60.

To summarize, Event 3 glass in the present study contains more reduced Fe and oxidized U in comparison with Events 1 and 2 glasses. The observed variation between melt glass samples from different events may be attributed to the differences in initial conditions, respective cooling rates, and/or the non-equilibrium redox conditions produced by a nuclear detonation. A nuclear explosion can produce an initial plasma largely devoid of oxygen (highly reducing conditions) and may mix metallic Fe from the device and/or associated structure with the oxidized Fe contained in the surrounding rock.[57] Recent studies have shown that some types of fallout such as aerodynamic fallout have likely quenched in the atmosphere within time scales of seconds.[54,56] We hypothesize that this

short cooling time scale inhibits the expected Fe/U buffering effect by locking in the oxidation states of Fe and U before local oxygen fugacity can have any significant

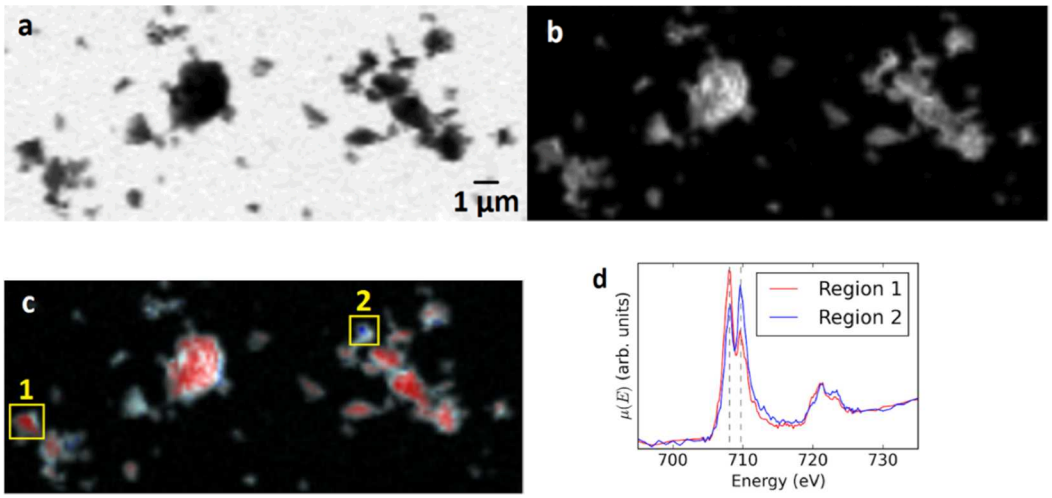

Figure 22. (a) Normal-contrast STXM image (at photon energy 745 eV) of nuclear test melt glass. (b) Fe elemental map. (c) Fe speciation map. Brightness indicates Fe content, while color represents the Fe^{2+}/Fe^{3+} ratio as determined from the branching ratio of the Fe L_3 edge. Red regions contain predominantly Fe^{2+} and blue regions contain predominantly Fe^{3+}. (d) Representative Fe L-edge spectra of the two regions indicated in (c). The peaks associated with Fe^{2+} (708 eV) and Fe^{3+} (709.7 eV) are marked.

effect (as in the production of synthetic glasses under equilibrium conditions). These effects must be disentangled to draw quantitative forensic conclusions regarding the sources of iron in the melt glass.

A natural next step is to study the spatial distribution of Fe and U species, with the goal of more precisely describing the Fe-U redox chemistry. SEM studies in the literature suggest that metallic inclusions can be found in the glass with sizes ranging from nanometers to microns,[57,65] and that STXM is therefore an ideal tool for this measurement.[66] To illustrate, Fig. 22 shows the distribution of Fe(II) and Fe(III) in a small sample of melt glass. No uranium or metallic Fe was detected in the particular sample chosen for STXM in this instance. Note that the bulk-averaged concentration of U in nuclear melt glass is typically below 50 µg/g,[56] which would be below the STXM transmission-mode detection limit if U were spread uniformly through the material.

IV.E. Software development results

A suite of software tools for efficient data acquisition and analysis have been developed and tested at the ALS-MES STXM beamline.[67] The first program developed for this purpose, "STXM Live," has two main functions. First, during STXM data acquisition, stacks of images are automatically processed into spectra in real time. This improves the efficiency of beam time by allowing the user to more readily detect possible errors (e.g., spectral "glitches" or drift in sample position during a long scan). For utility to the broader STXM community, files are also generated in formats compatible with the

commonly used aXis2000 analysis software package.[68] Second, a search function can suggest subregions of a large low-resolution image to be further inspected at high resolution. The user must provide a set of previously acquired images of samples whose morphologies are expected to be similar to the current sample. These are used to generate a statistical description of the likely spatial distribution of material, including variations in elemental composition. In particular, the program attempts to estimate the typical distance between large particles (which can be detected in low-resolution images) and submicron-scale particles (not detected in low-resolution images, but necessary for acquisition of reliable absorption spectra). This estimate is then applied to images as the user acquires them, and the results are displayed on request. This functionality is expected to improve the throughput of STXM for forensic specimens by reducing the time needed to fully characterize a highly heterogeneous sample.

Two additional applications have recently been developed that may be used either in conjunction with STXM Live or independently. "STXM Log" automatically generates an easily-readable log file summarizing activity on the instrument. "STXM Fingerprint" compares absorption spectra with a user-provided collection of data on reference materials. Automatic background-removal[69] and peak-fitting routines are used to quantitatively characterize newly acquired spectra and determine the most likely match in the reference dataset (Fig. 24). This extension has clear utility for forensic studies.

V. Future prospects

V.A. Other forensic specimens of interest

The capabilities of STXM, sample preparation and data acquisition protocols have been established and demonstrated to be amenable to a wide range of future nuclear forensic studies, especially on materials consisting of small particles and/or materials with small-scale heterogeneities. Interesting candidates for STXM analysis include transuranic materials, nuclear fuel cycle materials, and in general, difficult heterogeneous specimens such as environmental or contaminated samples. Ongoing discussions with members of the forensics community have identified several classes of materials for which spectromicroscopy is likely to provide unique and essential information to complement existing data.

V.B. Ptychography

The necessary equipment to conduct ptychography (diffraction-enhanced STXM imaging and spectroscopy) with highly radioactive materials to reach the true nanoscale (approaching 3 nm) spatial resolution for nuclear materials studies has been commissioned at the ALS.[70] However, the installation of dedicated beamline ptychography apparatus in the MES STXM has been delayed resulting from several complications and thus, there has not been an opportunity to conduct ptychography experiments with forensic types of materials The experimental assurance-testing infrastructure for many classes of nuclear forensic specimens is straightforward, and will be put in place to enable characterization by ptychography. This capability will allow the

examination of single environmental particles that approach the true nanoscale down to about 3 nm, such as aerosols, colloids, and particles. This would present new opportunities for improved chemical imaging with better spatial resolution.

V.C. Access to STXM

A consideration for nuclear forensics is the availability of the MES STXM beam time (or other STXM) to prioritize analysis of a nuclear forensic specimen (for example, following a seizure of illicit material) or as a sustained part of a long-term campaign. The availability of the MES STXM at the ALS is compatible with these scenarios as several access modes (including rapid access) are available. The nuclear forensics analysis timeline set forth by the International Atomic Energy Agency for a similar analysis technique, TEM, is frequently quoted at two months. This is well within the capabilities of the MES STXM (unless the timing coincides with one of the planned shutdowns of the ALS storage ring for upgrades). A programmatic stepping-stone for nuclear forensics with the STXM in the near future will be the participation in collaborative analyses of a single sample across multiple laboratories, which may test access to the MES STXM.

In the near term, the continued development of soft X-ray beamline capabilities (as well as intermediate X-rays) to enhance types of data with utility for nuclear forensics will develop a baseline for use and rapid access for high-priority samples. In the longer term, the development of a laboratory-based instrument would enable further improvements in sample analysis and turnaround times. New developments in dedicated facility laboratory-based X-ray light sources (laser wakefield, plasma sources, and inverse Compton scattering accelerators) coupled to new detector technologies, particularly in the soft and intermediate X-ray regions, offer promise for developing these capabilities in the future. The flexibility of the technique has potential greatly improve, as it will become possible to acquire data in locations outside of synchrotron light source facilities (for example, in situations where maintaining control over sample material is of high concern).

VI. Conclusion

The soft X-ray MES STXM at Beamline 11.0.2 STXM has been successfully demonstrated for characterization of materials such as those of interest to nuclear forensics including the non-destructive, analytical speciation of small radioactive particles and materials and heterogeneous materials. The technical development of the MES STXM for nuclear forensics studies has resulted in significant performance improvements in fluorescence detection, sample identification/handling, and the STXM data acquisition and control system. An attractive part of STXM is its nondestructive nature, and its ability to avoid sample damage during data collection. Nuclear forensics studies at the MES STXM have examined material signatures using XANES from actinide materials at the $N_{4,5}$-edges, from light atom constituents at the K-edges, and other relevant X-ray absorption edges residing in the soft X-ray region. As part of the suite of analytical methods used in forensic studies, the unique benefits of STXM include the spectroscopic signature information it provides (allowing identification of amorphous

materials) and its sensitivity to light elements that are not easily detectable by other conventional methods such as mass spectrometry.

A library of soft X-ray absorption spectra from a broad range of uranium materials has been compiled for future reference against unidentified forensic specimens. Several interdicted specimens have been examined by STXM, revealing micron-scale variations in oxidation state in one specimen, and detecting carbon contamination in all three specimens. Uranium oxides aged under controlled conditions have been studied by intermediate-energy and oxygen K-edge XANES, identifying layers and inclusions of various oxide phases and schoepite. The redox states of several nuclear melt glasses have been determined by hard X-ray spectroscopy, revealing possible time-dependent quenching effects; FIB/STXM studies in this direction are ongoing.

These soft X-ray STXM spectromicroscopy results have provided insightful data complementary to the elemental, isotopic, and morphological data provided from existing nuclear forensic techniques. There is room for continued ongoing technical improvement of STXM to further optimize its capabilities for nuclear forensics studies. Most importantly, the capabilities of soft X-ray STXM for conducting scientific nuclear forensic studies on materials of interest and on real specimens have been demonstrated. Integration with existing forensic efforts will be key for STXM to become more familiar to the forensics community, to establish collaborative relationships, and to share strategic specimens. From these results, it is evident that soft X-ray and intermediate X-ray spectromicroscopy can make valuable contributions to the field of nuclear forensics.

The information obtained from these studies has shown that further development and application of synchrotron radiation techniques, particularly in the soft X-ray regime (as well as intermediate-energy X-rays), has significant potential for contributions to nuclear forensics. The results of this research indicate that future development of specialized beamline and laboratory-based facilities with either soft or intermediate-energy X-ray spectromicroscopy capabilities would have significant beneficial impact for nuclear forensics. For example, nuclear materials characterization may benefit from the implementation and development of ptychography.

VII. Acknowledgments

We thank Pat Allen and Tim Rose for useful insights and discussion of the hard X-ray data, and thank Petrus Zwart for the loan of the detector used for intermediate-energy XES and HR-XANES.

This work was supported by the NNSA Office of Defense Nuclear Nonproliferation R&D (NA-22) of the U.S. Department of Energy (DOE) under Contract Number DE-AC02-05CH11231 at Lawrence Berkeley National Laboratory (LBNL) (JIP, CHB, DKS) and under Contract Number DE-AC52-07NA27344 at Lawrence Livermore National Laboratory (KBK, KSH, MJK). Research at the Molecular Environmental Science Beamline 11.0.2 at the ALS was supported by the Director, Office of Science, Office of Basic Energy Sciences, Division of Chemical Sciences, Geosciences, and Biosciences

Condensed Phase and Interfacial Molecular Sciences Program of the U.S. DOE at LBNL under Contract No. DE-AC02-05CH11231. SGM was supported by the Director, Office of Science, Office of Basic Energy Sciences, Division of Chemical Sciences, Geosciences, and Biosciences Heavy Element Chemistry Program of the U.S. DOE at LBNL under Contract No. DE-AC02-05CH11231. The ALS and TT were supported by the Director, Office of Science, Office of Basic Energy Sciences, of the U.S. DOE under Contract No. DE-AC02-05CH11231 at LBNL. ABA acknowledges support by a DOE Integrated University Program Fellowship at the University of California, Berkeley. Use of SSRL, SLAC National Accelerator Laboratory, is supported by the U.S. Department of Energy, Office of Science, Office of Basic Energy Sciences under Contract No. DE-AC02-76SF00515. LLNL-TR-704343.

VIII. References

[1] M. J. Kristo and S. J. Tumey, *Nuclear Instruments and Methods in Physics Research, Section B: Beam Interactions with Materials and Atoms* **294,** 656 (2013).

[2] K. Mayer, M. Wallenius, and Z. Varga, *Chemical Reviews* **113,** 884 (2013).

[3] K. J. Moody, I. D. Hutcheon, and P. M. Grant, *Nuclear Forensic Analysis*, 2nd ed. (CRC Press, Boca Raton, FL, 2015).

[4] K. Mayer, M. Wallenius, K. Lützenkirchen, J. Galy, Z. Varga, N. Erdmann, R. Buda, J.-V. Kratz, N. Trautmann, and K. Fifield, *Journal of Physics: Conference Series* **312,** 062003 (2011).

[5] K. Mayer, M. Wallenius, and I. Ray, *The Analyst* **130,** 433 (2005).

[6] M. Wallenius, K. Lützenkirchen, K. Mayer, I. Ray, L. A. de las Heras, M. Betti, O. Cromboom, M. Hild, B. Lynch, A. Nicholl, H. Ottmar, G. Rasmussen, A. Schubert, G. Tamborini, H. Thiele, W. Wagner, C. Walker, and E. Zuleger, *Journal of Alloys and Compounds* **444-445,** 57 (2007).

[7] P. M. Grant, K. J. Moody, I. D. Hutcheon, D. L. Phinney, R. E. Whipple, J. S. Haas, A. Alcaraz, J. E. Andrews, G. L. Klunder, R. E. Russo, T. E. Fickies, G. E. Pelkey, B. D. Andresen, D. A. Kruchten, and S. Cantlin, *Journal of Radioanalytical and Nuclear Chemistry* **235,** 129 (1998).

[8] P. M. Grant, K. J. Moody, I. D. Hutcheon, D. L. Phinney, J. S. Haas, A. M. Volpe, J. J. Oldani, R. E. Whipple, N. Stoyer, A. Alcaraz, J. E. Andrews, R. E. Russo, G. L. Klunder, B. D. Andresen, and S. Cantlin, *Journal of Forensic Science***,** 680 (1998).

[9] M. Wallenius, K. Mayer, and I. Ray, *Forensic Science International* **156,** 55 (2006).

[10] E. Keegan, M. J. Kristo, M. Colella, M. Robel, R. Williams, R. Lindvall, G. Eppich, S. Roberts, L. Borg, A. Gaffney, J. Plaue, H. Wong, J. Davis, E. Loi, M. Reinhard, and I. Hutcheon, *Forensic Science International* **240,** 111 (2014).

[11] M. J. Kristo, E. Keegan, M. Colella, R. Williams, R. Lindvall, G. Eppich, S. Roberts, L. Borg, A. Gaffney, J. Plaue, K. Knight, E. Loi, M. Hotchkis, K. Moody, M. Singleton, M. Robel, and I. Hutcheon, *Radiochimica Acta* **103,** 487 (2015).

[12] J. J. Bellucci, A. Simonetti, C. Wallace, E. C. Koeman, and P. C. Burns, *Analytical Chemistry* **85,** 7588 (2013).

[13] J. J. Bellucci, A. Simonetti, C. Wallace, E. C. Koeman, and P. C. Burns, *Analytical Chemistry* **85,** 4195 (2013).

[14] M. C. Duff, J. U. Coughlin, and D. B. Hunter, *Geochimica et Cosmochimica Acta* **66,** 3533 (2002).

[15] N. J. Hess, W. J. Weber, and S. D. Conradson, *Journal of Nuclear Materials* **254,** 175 (1998).

[16] P. Jollivet, C. D. Auwer, and E. Simoni, *Journal of Nuclear Materials* **301,** 142 (2002).

[17] J. I. Pacold, M. J. Kristo, T. Tylisczcak, and D. K. Shuh, *(to be submitted)* (2016).

[18] D. E. Crean, F. R. Livens, M. C. Stennett, D. Grolimund, C. N. Borca, and N. C. Hyatt, *Environmental Science & Technology* **48,** 1467 (2014).

[19] I. M. Kempson, K. Paul Kirkbride, W. M. Skinner, and J. Coumbaros, *Talanta* **67,** 286 (2005).

[20] A. L. Tamasi, K. S. Boland, K. Czerwinski, J. K. Ellis, S. A. Kozimor, R. L. Martin, A. L. Pugmire, D. Reilly, B. L. Scott, A. D. Sutton, G. L. Wagner, J. R. Walensky, and M. P. Wilkerson, *Analytical Chemistry* **87,** 4210 (2015).
[21] G. Giuli, G. Pratesi, S. G. Eeckhout, and E. Paris, *Large Meteorite Impacts and Planetary Evolution IV* **465** (2010).
[22] T. P. Rose, a. B. Kersting, L. J. Harris, G. B. Hudson, D. K. Smith, R. W. Williams, D. R. Loewen, E. J. Nelson, and J. E. Moran, "Hydrologic Resources Management Program and Underground Test Area Project FY 2001 – 2002 Progress Report," (2003).
[23] M. Betti, G. Tamborini, and L. Koch, *Analytical Chemistry* **71,** 2616 (1999).
[24] X. Hou, W. Chen, Y. He, and B. T. Jones, *Applied Spectroscopy Reviews* **40,** 245 (2005).
[25] Y. Ranebo, M. Eriksson, G. Tamborini, N. Niagolova, O. Bildstein, and M. Betti, *Microscopy and Microanalysis* **13,** 179 (2007).
[26] G. Tamborini, *Microchimica Acta* **145,** 237 (2004).
[27] G. Tamborini, D. Phinney, O. Bildstein, and M. Betti, *Analytical Chemistry* **74,** 6098 (2002).
[28] G. Tamborini, M. Wallenius, O. Bildstein, L. Pajo, and M. Betti, *Microchimica Acta* **139,** 185 (2002).
[29] E. I. Solomon, B. Hedman, K. O. Hodgson, A. Dey, and R. K. Szilagyi, *Coordination Chemistry Reviews* **249,** 97 (2005).
[30] J. D. Ward, M. Bowden, C. T. Resch, S. Smith, B. K. McNamara, E. C. Buck, G. C. Eiden, and A. M. Duffin, *Geostandards and Geoanalytical Research* **40,** 135 (2015).
[31] S. G. Minasian, J. M. Keith, E. R. Batista, K. S. Boland, D. L. Clark, S. a. Kozimor, R. L. Martin, D. K. Shuh, and T. Tyliszczak, *Chemical Science* **5,** 351 (2014).
[32] X.-D. Wen, M. W. Löble, E. R. Batista, E. Bauer, K. S. Boland, A. K. Burrell, S. D. Conradson, S. R. Daly, S. a. Kozimor, S. G. Minasian, R. L. Martin, T. M. McCleskey, B. L. Scott, D. K. Shuh, and T. Tyliszczak, *Journal of Electron Spectroscopy and Related Phenomena* **194,** 81 (2014).
[33] H. Bluhm, K. Andersson, T. Araki, K. Benzerara, G. E. Brown, J. J. Dynes, S. Ghosal, M. K. Gilles, H. C. Hansen, J. C. Hemminger, A. P. Hitchcock, G. Ketteler, a. L. D. Kilcoyne, E. Kneedler, J. R. Lawrence, G. G. Leppard, J. Majzlam, B. S. Mun, S. C. B. Myneni, a. Nilsson, H. Ogasawara, D. F. Ogletree, K. Pecher, M. Salmeron, D. K. Shuh, B. Tonner, T. Tyliszczak, T. Warwick, and T. H. Yoon, in *Soft X-ray microscopy and spectroscopy at the molecular environmental science beamline at the Advanced Light Source*, 2004, p. 86.
[34] A. L. D. Kilcoyne, T. Tyliszczak, W. F. Steele, S. Fakra, P. Hitchcock, K. Franck, E. Anderson, B. Harteneck, E. G. Rightor, G. E. Mitchell, A. P. Hitchcock, L. Yang, T. Warwick, and H. Ade, *Journal of Synchrotron Radiation* **10,** 125 (2003).
[35] T. Tyliszczak, in *Soft X-ray Scanning Transmission Microscope Working in an Extended Energy Range at the Advanced Light Source*, 2004, p. 1356.
[36] F. M. F. de Groot, E. de Smit, M. M. van Schooneveld, L. R. Aramburo, and B. M. Weckhuysen, *Chemphyschem* **11,** 951 (2010).
[37] C. A. Volkert and A. M. Minor, *MRS Bulletin* **32,** 389 (2007).
[38] J. Petiau, G. Calas, D. Petitmaire, A. Bianconi, M. Benfatto, and A. Marcelli, *Physical Review B* **34,** 7350 (1986).

[39] S. M. Butorin, *Journal of Electron Spectroscopy and Related Phenomena* **110,** 213 (2000).
[40] P. Glatzel, T.-C. Weng, K. Kvashnina, J. Swarbrick, M. Sikora, E. Gallo, N. Smolentsev, and R. A. Mori, *Journal of Electron Spectroscopy and Related Phenomena* **188,** 17 (2013).
[41] K. Kvashnina, S. Butorin, P. Martin, and P. Glatzel, *Physical Review Letters* **111,** 253002 (2013).
[42] B. A. Mattern, G. T. Seidler, M. Haave, J. I. Pacold, R. A. Gordon, J. Planillo, J. Quintana, and B. Rusthoven, *The Review of Scientific Instruments* **83,** 023901 (2012).
[43] J. I. Pacold, J. A. Bradley, B. A. Mattern, M. J. Lipp, G. T. Seidler, P. Chow, Y. Xiao, E. Rod, B. Rusthoven, and J. Quintana, *Journal of Synchrotron Radiation* **19,** 245 (2012).
[44] A. Walshe, T. Prüßmann, T. Vitova, and R. J. Baker, *Dalton Transactions* **43,** 4400 (2014).
[45] P. G. Allen, D. K. Shuh, J. J. Bucher, N. M. Edelstein, T. Reich, M. A. Denecke, and H. Nitsche, *Inorganic Chemistry* **35,** 784 (1996).
[46] P. G. Allen, D. K. Shuh, J. J. Bucher, N. M. Edelstein, C. E. A. Palmer, R. J. Silva, S. N. Nguyen, L. N. Marquez, and E. A. Hudson, *Radiochimica Acta* **75,** 47 (1996).
[47] H. J. Nilsson, T. Tyliszczak, R. E. Wilson, L. Werme, and D. K. Shuh, *Analytical and Bioanalytical Chemistry* **383,** 41 (2005).
[48] P. Maldonado, L. Z. Evins, and P. M. Oppeneer, *The Journal of Physical Chemistry C* **118,** 8491 (2014).
[49] R. J. McEachern and P. Taylor, *Journal of Nuclear Materials* **254,** 87 (1998).
[50] G. Rousseau, L. Desgranges, F. Charlot, N. Millot, J. C. Nièpce, M. Pijolat, F. Valdivieso, G. Baldinozzi, and J. F. Bérar, *Journal of Nuclear Materials* **355,** 10 (2006).
[51] S. D. Senanayake, G. I. N. Waterhouse, A. S. Y. Chan, T. E. Madey, D. R. Mullins, and H. Idriss, *Journal of Physical Chemistry C* **111,** 7963 (2007).
[52] J. E. Stubbs, A. M. Chaka, E. S. Ilton, C. A. Biwer, M. H. Engelhard, J. R. Bargar, and P. J. Eng, *Physical Review Letters* **114,** 1 (2015).
[53] S. Glasstone and P. Dolan, *The Effects of Nuclear Weapons*, United States Department of Deense and the Energy Research and Development Administration, Washington, DC, 1977.
[54] W. S. Cassata, S. G. Prussin, K. B. Knight, I. D. Hutcheon, B. H. Isselhardt, and P. R. Renne, *Journal of Environmental Radioactivity* **137C,** 88 (2014).
[55] A. B. Kersting, *Inorganic Chemistry* **52,** 3533 (2013).
[56] G. R. Eppich, K. B. Knight, T. W. Jacomb-Hood, G. D. Spriggs, and I. D. Hutcheon, *Journal of Radioanalytical and Nuclear Chemistry* **302,** 593 (2014).
[57] A. J. Fahey, C. J. Zeissler, D. E. Newbury, J. Davis, and R. M. Lindstrom, *Proceedings of the National Academy of Sciences* **107,** 20207 (2010).
[58] J. J. Bellucci, A. Simonetti, E. C. Koeman, C. Wallace, and P. C. Burns, *Chemical Geology* **365,** 69 (2014).
[59] E. C. Koeman, A. Simonetti, and P. C. Burns, *Analytical Chemistry* **87,** 5380 (2015).
[60] J. I. Pacold, W. W. Lukens, C. H. Booth, D. K. Shuh, K. B. Knight, G. R. Eppich, and K. S. Holliday, *Journal of Applied Physics* **119,** 195102 (2016).

[61] H. D. Schreiber, *Journal of the Less Common Metals* **91,** 129 (1983).
[62] H. D. Schreiber, *Journal of Non-Crystalline Solids* **42,** 175 (1980).
[63] H. D. Schreiber, B. K. Kochanowski, C. W. Schreiber, A. B. Morgan, M. T. Coolbaugh, and T. G. Dunlap, *Journal of Non-Crystalline Solids* **177,** 340 (1994).
[64] G. Calas, *Geochimica et Cosmochimica Acta* **43,** 1521 (1979).
[65] G. N. Eby, N. Charnley, D. Pirrie, R. Hermes, J. Smoliga, and G. Rollinson, *American Mineralogist* **100,** 427 (2015).
[66] F. Bourdelle, K. Benzerara, O. Beyssac, J. Cosmidis, D. R. Neuville, G. E. Brown, and E. Paineau, *Contributions to Mineralogy and Petrology* **166,** 423 (2013).
[67] J. I. Pacold, Sep 2016 ed. (2016).
[68] A. P. Hitchcock, Apr 2016 ed. (2016).
[69] T.-C. Weng, G. S. Waldo, and J. E. Penner-Hahn, *Journal of Synchrotron Radiation* **12,** 506 (2005).
[70] D. A. Shapiro, Y.-S. Yu, T. Tyliszczak, J. Cabana, R. Celestre, W. Chao, K. Kaznatcheev, A. L. D. Kilcoyne, F. Maia, S. Marchesini, Y. S. Meng, T. Warwick, L. L. Yang, and H. A. Padmore, *Nature Photonics***,** 1 (2014).

Appendix 1: List of Tables and Figures

Figure 14. High-resolution U M_5-edge XANES spectra acquired from a reference uranium oxide powder and aged UO_2 samples.

Figure 15. Normal contrast image (left) and uranium map (right) of a FIB section extracted from UO2 aged for 90 days at 98% relative humidity. Note that a layer of Pt was applied during the FIB process.

Figure 16. Oxygen K-edge spectra acquired from the FIB section shown in Fig. 12 at several depths from the surface.

Figure 17. Normal contrast image (left) and uranium map (right) of a FIB section extracted from UO_2 aged for 378 days at 98% relative humidity.

Figure 18. Spectromicroscopic analysis of the FIB section shown in Fig. 14. (a) Detail of Fig. 17(a). (b) Oxygen K-edge spectra acquired from near-surface and bulk regions indicated in (a). (c) False-color image colored by the intensity of the absorption peak at 531 eV.

Figure 19. U L3-edge XANES acquired from melt glass specimens and reference U materials. By interpolating between the positions of the peaks corresponding to the U(IV) and U(IV) standards UO_2 and $UO_2(CH_3COO)_2$, it is possible to estimate the average oxidation state of uranium in each melt glass specimen (+4.6 for the Event 1 glass; +4.7 for the Event 2 glass; and +5.7 for the Event 3 glass).

Figure 20. Fe K-edge XANES acquired from melt glass specimens and reference Fe materials. By interpolating between the positions of the Fe K edge at half-height for FeO and Fe_2O_3, it is possible to estimate the average oxidation state of Fe in each material (+3.0 for the soils; +2.2 for the Event 1 glass; +2.1 for the Event 2 glass; and +1.9 for the Event 2 glass).

Figure 21. Fourier-transformed U L_{III}-edge EXAFS data and fit results for the Event 3 melt glass. The fit results indicate that ~60% of the uranium in the specimen is in uranyl-like coordination; more details are given in ref. 60.

Figure 22. (a) Normal-contrast STXM image (at photon energy 745 eV) of nuclear test melt glass. (b) Fe elemental map. (c) Fe speciation map. Brightness indicates Fe content, while color represents the Fe^{2+}/Fe^{3+} ratio as determined from the branching ratio of the Fe L_3 edge. Red regions contain predominantly Fe^{2+} and blue regions contain predominantly Fe^{3+}. (d) Representative Fe L-edge spectra of the two regions indicated in (c). The peaks associated with Fe^{2+} (708 eV) and Fe^{3+} (709.7 eV) are marked.

Appendix 2: Scientific and Collaborative Activities

The LBNL STXM team participated in and made a short STXM presentation entitled "Analysis of Thin Sections of Aged UO_2", in the Schubert Review of the Davisson NNSA Project at LLNL on 30 June 2016. The LBNL STXM team also used this opportunity to interact with team members and collaborators on ongoing NNSA projects.

A Davisson postdoctoral fellow, Scott Donald, was trained for ALS and participated in beam time during STXM analysis of aged UO_2 powders.

The LBNL team hosted a productive half-day meeting with potential collaborators from LLNL (Lee Davisson, Art Nelson) to discuss scientific interests with nuclear forensics, capabilities, and areas of possible collaboration. This interaction was extremely fruitful and the LBNL and LLNL teams made plans to conduct a set of STXM experiments on series of aged uranium oxides in late January of 2016. Part of the LLNL team also includes Rod Ewing of Stanford University and an in person discussion was held during a fortuitous travel encounter.

The LBNL team worked with Andrew Duffin of PNNL to support nuclear forensic experiments with STXM and bulk X-ray absorption experiments at the ALS (2015-2014).

A visit to LLNL was made on September 29, 2015 to discuss results.

The Schubert Review of the LBNL project was held in June of 2015.

There was follow up visit after the seminar at LLNL to speak with researchers (Kevin Roberts) about the possibility of receiving specimens of interest for nuclear forensic research.

Co-organized the "Soft X-ray Science and Light Source Developments for Actinide Science," workshop at the October 2014 SSRL SLAC User Meeting on synchrotron radiation science that included a nuclear forensics session. Encouraged and sponsored presentations by several nuclear forensics researchers utilizing synchrotron radiation.

Performed a peer review for a nuclear forensics manuscript submitted to Analytical Chemistry.

Beam Time Proposals Supporting This Research

A new Approved Program (AP) user proposal was submitted to the ALS in January 2016 for renewed long-term access to the Molecular Environmental Science (MES) beamline 11.0.2 STXM. The proposal was successful and received a competitive score that will enable sufficient STXM access beginning in July 2016 for two years.

Publications and Publications in Preparation

J. I. Pacold, W. W. Lukens, C. H. Booth, D. K. Shuh, K. B. Knight, G. R. Eppich, and K. S. Holliday, "Chemical Speciation of Uranium, Iron, and Plutonium in Melt Glass From Nuclear Weapons Testing," J. Appl. Phys. **119**, 195102 (2016); DOI: 10.1063/1.4948942.

J. I. Pacold, A. Altman, C. H. Booth, S. G. Minasian, T. Tyliszczak, D. K. Shuh, "Development of Small Particle Speciation for Nuclear Forensics by Soft X-ray Scanning Transmission Spectromicrosopy," The Analyst, to be submitted (2017).

J. I. Pacold, M. Kristo, T. Tyliszczak, and D. K. Shuh, "Soft X-ray Spectromicroscopy Analysis of Interdicted Uranium Materials," to be submitted (2017).

J. I. Pacold, T. Tyliszczak, and D. K. Shuh, "Accelerated Data Acquisition Method for the Statistical Location of Particles of Interest for Scanning Transmission X-ray Microscopy", Microscopy and Microanalysis, in preparation (2017).

S. M. Donald, J. I. Pacold, Z. Dai, A. J. Nelson, D. K. Shuh, and M. L. Davisson, "Spectroscopic Characterization of Controlled Aging of UO_2", in preparation (2017).

Presentations

A nuclear forensics abstract entitled "Spatially Resolved Uranium Speciation by Scanning Transmission X-ray Microscopy in Nuclear Materials," was submitted to the American Vacuum Society (AVS) 63rd International Symposium and Exhibit to be held in Nashville, TN from 6-11 November 2016.

The applications of synchrotron radiation to nuclear forensics were included in the lectures given to the American Chemical Society Nuclear Science Summer School at San Jose State University (28 June 2016) and in the Chemistry 208 guest lecture at UC Berkeley (25 April 2016).

An unclassified presentation entitled "Small Particle Speciation for Forensic Analysis by Soft X-ray Scanning Transmission Microscopy," was given by D. K. Shuh at the Nuclear Forensics Program Meeting in Albuquerque, NM on 5 April 2016.

J. Pacold (LBNL postdoctoral researcher) gave a contributed presentation in the MRS Nuclear Forensics session entitled "Forensic Analysis of Uranium Materials by Scanning Transmission X-ray Microscopy."

There was a day long visit to NA20 and a presentation given at NA20 on 1 October 2015 in Washington D.C. entitled "Soft X-ray Spectromicroscopy for Small Particle Nuclear Forensic Analysis." This was a particularly enlightening and informative visit (accompanied by John Valentine, LBNL Lab Program Manager).

Postdoctoral fellow (Pacold) gave a presentation at American Chemical Society Fall 2015 National Meeting in Boston entitled "Determination of the Spatial Distribution and Chemical State of Radionuclides in Model Samples" and attended the Nuclear Chemistry and Technology Division (NUCL) session on Nuclear Forensics (3 days).

Invited seminar entitled "Soft X-ray Spectromicroscopy for Small Particle Forensic Analysis" in the Nuclear Forensics Seminar Series in the Department of Nuclear Engineering and Radiological Sciences at Oregon State University, 12 March 2015.

A seminar entitled "Soft X-ray Spectromicroscopy of Actinide Materials" was given at LLNL, 18 August 2014.

D. K. Shuh gave a seminar entitled "Soft X-ray Spectromicroscopy of Actinide Materials" at the Institute of Chemistry-Nice, University of Nice Sophia Antipolis, Nice, France, 24 June 2014.

J. Valentine gave a seminar entitled "Small Particle Speciation for Forensic Analysis by Soft X-ray Scanning Transmission X-ray Microscopy" at the FY14 Joint Program Review Meeting, NA-22 Nuclear Forensics Projects, Los Alamos, NM, June 18 2014.